AIP | Applied Physics Letters

Improving the sensitivity of a near-infrared nanocomposite photodetector by enhancing trap induced hole injection

Liang Shen, Yanjun Fang, Qingfeng Dong, Zhengguo Xiao, and Jinsong Huang

Citation: Applied Physics Letters **106**, 023301 (2015); doi: 10.1063/1.4905930
View online: http://dx.doi.org/10.1063/1.4905930
View Table of Contents: http://scitation.aip.org/content/aip/journal/apl/106/2?ver=pdfcov
Published by the AIP Publishing

Improving the sensitivity of a near-infrared nanocomposite photodetector by enhancing trap induced hole injection

Liang Shen, Yanjun Fang, Qingfeng Dong, Zhengguo Xiao, and Jinsong Huang[a)]
Department of Mechanical and Materials Engineering and Nebraska Center for Materials and Nanoscience, University of Nebraska–Lincoln, Lincoln, Nebraska 68588-0656, USA

(Received 7 December 2014; accepted 4 January 2015; published online 12 January 2015)

We report the enhancement of the photoconductive gain of nanocomposite near-infrared photodetectors by a zinc oxide nanoparticles (ZnO NPs) rich surface at the nanocomposite/cathode interface. An argon plasma etching process was used to remove polymer at the surface of nanocomposite films, which resulted in a ZnO NPs rich surface. The other way is to spin-coat a thin layer of ZnO NPs onto the nanocomposite layer. The ZnO NPs rich surface, which acts as electron traps to induce secondary hole injection under reverse bias, increased hole injection, and thus the external quantum efficiency by 2–3 times. The darkcurrent declined one order of magnitude simultaneously as a result of etching the top nanocomposite layer. The specific detectivity at 800 nm was increased by 7.4 times to 1.11×10^{10} Jones due to the simultaneously suppressed noise and enhanced gain. © *2015 AIP Publishing LLC*. [http://dx.doi.org/10.1063/1.4905930]

Near-infrared (NIR) photodetectors have broad applications in optical imaging, telecommunications, medical imaging, and environmental monitoring.[1–6] Since 2000, along with the rapid development of semiconducting polymer research, the polymer-based photodetectors have attracted more and more attentions due to their advantages of light weight, flexibility, and low-cost compared to traditional crystalline semiconductor based photodetectors.[7–11] The low free carrier concentration in intrinsic organic semiconducting materials combining with the charge blocking layers provides a mechanism to achieve a low noise current in polymer photodetectors despite of the existence of a large density of defects in these materials.[12–15] Recent rapid development in low-bandgap materials for polymer solar cell applications also provides many choices of materials for NIR photodetectors.[16–18]

A sensitive photodetector needs to have a large responsivity. However, most of reported polymer photodetectors work as photodiodes which do not have a gain. Recently, we developed a type of solution-processed nanocomposite photodetector with active layers of inorganic zinc oxide nanoparticles (ZnO NPs) blended with poly(3-hexylthiophene) (P3HT) or polyvinylcarbazole (PVK), which displayed an ultrahigh gain originated from an interfacial trap-triggered secondary charge injection.[12] The high gain of device under illumination and low noise current in dark in these nanocomposite devices supply a mechanism to increase detectivity or sensitivity of photodetectors. We extended the response spectrum to NIR range by introducing lead sulfide (PbS), which is a NIR absorber, into the nanocomposite layer and increased the external quantum efficiency (EQE) in the NIR range to above 100% by utilizing the charge traps in ZnO NPs for a photoconductive gain and photo-induced charge transfer from PbS to ZnO NPs.[14] In this work, we directly combine ZnO NPs with a NIR absorbing semiconducting polymer to develop high gain NIR nanocomposite photodetectors. Here, we employed a surface treatment method to enhance trap induced holes injection, which increased the gain of the photodetectors by ~2.5 times, and increased the specific detectivity of the NIR photodetectors to 1.11×10^{10} Jones.

The idea of generating a nanoparticle richer top surface in the nanocomposite films to enhance the photoconductive gain of the photodetectors is illustrated by the energy diagram shown in Fig. 1. The bulk heterojunction active layer, which is composed of nanoparticles and a semiconducting polymer, can absorb incident photons and generate Frenkel excitons under illumination. Due to the large energy offset, the generated excitons are separated at the interface of the polymer and nanoparticles. The holes are transported away through the semiconducting polymer, but the electrons are trapped by the nanoparticles due to the intentionally designed nanoparticles with a large density of electron traps at the surface of the nanoparticles. In our device design, the trapped electrons in nanoparticles, which are generated by incident photons, can trigger on the secondary hole injection under reverse bias, because the trapped electrons cause the band-bending in the region close to the cathode side. This suggests that the degree of the energy level bending is dependent on the density of nanoparticles. As illustrated in Figure 1, richer nanoparticles at the cathode side can cause a sharper energy band bending, which enhances the secondary charge injection and thus the gain of the photodetectors.

Poly[2,7-(5,5-bis-(3,7-dimethyloctyl)-5H-dithieno[3,2-b:2′,3′-d]pyran)-alt-4,7-(5,6-difluoro-2,1,3-benzothia diazole)] (PDTP-DFBT) was chosen as the semiconductor light absorber.[19] It is suitable as the light absorber in NIR photodetector owing to its broad absorption spectrum from 300 nm to 900 nm, and especially a strong absorption peak at 800 nm. The NIR-photodetector fabrication method is schematically shown in Figs. 2(a) and 2(b). Poly(3,4-ethylenedioxythiophene) poly(styrenesulphonate)(PEDOT:PSS) was first spin-coated onto a indium tin oxide(ITO)-conducting glass substrate as an anode modified layer. The blend of

[a)]Author to whom correspondence should be addressed. Electronic mail: jhuang2@unl.edu. Telephone: +1−(402)−472-2640.

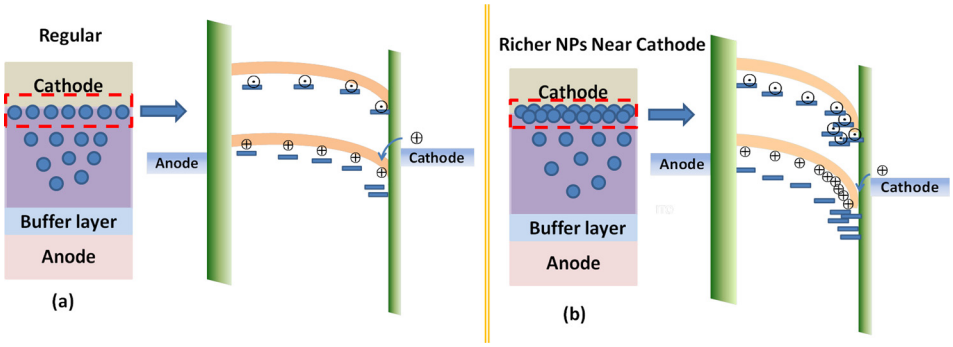

FIG. 1. Energy level bending comparison between the nanoparticle regular (a) and richer (b) top surface in the nanocomposite films.

PVK and 4, 4′-bis[(p-trichlorosilylpropylphenyl) phenylamino]-bipheny (TPD-Si_2) was spin-coated on the top of PEDOT:PSS film surface as a hole-transport but electron-blocking layer. Then, the samples were annealed in air to crosslink TPD-Si_2. The photoactive layer, which was composed of ZnO NPs and PDTP-DFBT blended at a weight ratio of 3:1, was spun and solvent-annealed to enhance the hole mobility. Then, the samples were etched by Ar plasma (PE-25 series plasma system) for 20–30 s to remove partial of the PDTP-DFBT polymer on the surface of the nanocomposite films and expose more ZnO NPs. Finally, the devices were finished by evaporating 2,9-dimethyl-4,7-diphenyl-1,10-phenanthroline (BCP) and Aluminum (Al). The blend ratio of ZnO NPs:PDTP-DFBT is 3:1 in weight, which is the optimized ratio for the best film morphology and a relatively high gain. Adding more ZnO NPs renders the film non-compact which increases the noise current, while reducing ZnO NPs loading lowers the total trap density and thus reduces the photoconductive gain. Figures 2(c)–2(f) show the atom force microscopy (AFM) topography and phase images of PDTP-DFBT:ZnO nanocomposite films before and after Ar plasma etching. It can be seen that the pristine PDTP-DFBT:ZnO NPs nanocomposite film was relatively flat with an average roughness of 5.1 nm. It can be seen from the figures that there is obvious contrast of phase between ZnO NPs and PDTP-DFBT. There are ZnO NPs and PDTP-DFBT at the nanocomposite surface before the Ar plasma etching. After Ar plasma etching, more ZnO NPs were exposed, and the average roughness increased to 5.6 nm. At the same time, ZnO NPs occupied most of the nanocomposite film surface, and PDTP-DFBT almost disappeared at the nanocomposite surface. It indicates that ZnO NPs are richer in the surface of PDTP-DFBT: ZnO NPs nanocomposite after Ar plasma etching, which is accorded with the idea of generating a nanoparticle richer top surface in the nanocomposite films.

The absorption spectra of ZnO NPs, PDTP-DFBT, and the blend of them are measured and shown in Fig. 3(a). It can be seen that PDTP-DFBT has three main absorption peaks with the strongest one at 800 nm. ZnO NPs have strong absorption in wavelength range between 300 nm and 360 nm, thus the ZnO NPs:PDTP-DFBT nanocomposite has a broad absorption band spanning from UV to NIR range.

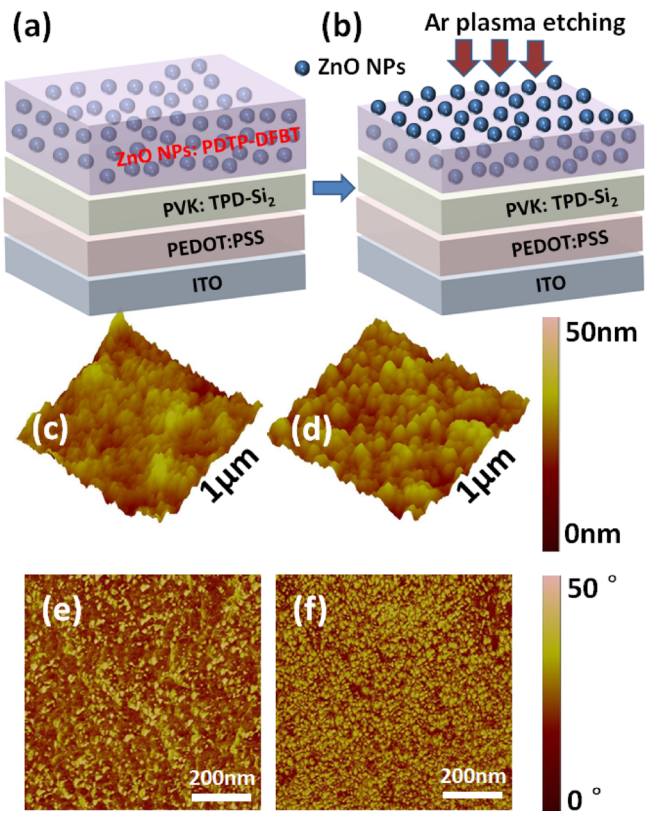

FIG. 2. Device fabrication process of the nanocomposite NIR-photodetector (a) before (b) after Ar plasma etching. AFM morphology and phase images of PDTP-DFBT: ZnO NPs nanocomposites surface before ((c) and (e)) after ((d) and (f)) Ar plasma etching.

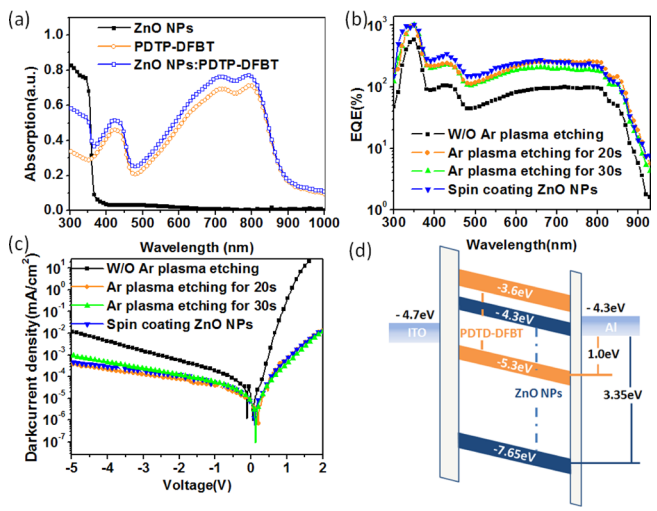

FIG. 3. (a) The absorption spectra of the ZnO NPs, PDTP-DFBT, and the blend of ZnO NPs and PDTP-DFBT. (b) EQE curve under illumination at −4.5 V reverse bias for all devices. (c) J–V characteristic curve in the dark at −4.5 V reverse bias for all devices. (d) The energy diagram of the nanocomposite NIR-photodetector in the dark under reverse bias.

We continued to evaluate the influence of plasma etching on the gain of the photodetectors. The presence of a gain in the devices was confirmed by EQE measurements with an incident photon-to-current efficiency (IPCE) system at −4.5 V reverse bias, and the results are shown in Fig. 3(b). The EQE of devices without Ar plasma etching is about 100% at 800 nm, which verified the photoconductive gain in our NIR photodetectors. As expected, after Ar plasma etching for 20 s, the EQE of devices at 800 nm at the same bias increased by 2.5 times to 248%. Further increasing Ar plasma etching time to 30 s, however, resulted in a declined EQE to 183% at 800 nm. It can be understood by the possible degradation of the semiconducting polymer caused by the too much Ar plasma etching, which reduced the hole injection from cathode to the polymer layer under reverse bias and/or damaged the transport property. The corresponding responsivity (R in A/W) for all the devices, which is the ratio of photocurrent density to the intensity of incident light, could be calculated according to the following equation to be 0.65 A/W, 1.60 A/W, and 1.18 A/W, respectively,

$$R = EQE/h\nu, \tag{1}$$

where $h\nu$ is the energy of the incident photon in electronvolt (eV). The observed higher EQE and R confirmed that the Ar plasma etching with appropriate etching time has increased the secondary hole injection significantly. Accordingly, the ZnO NP richer nanocomposite/Al interface acts as a sensitive photon-addressable optoelectronic "valve" for hole injection and incident photons can switch on this valve. The average energy barrier change of Schottky junction, $\Delta\varphi$, is a linear function of trapped electron density n_t by ZnO NPs, while the injection hole number follows an exponential relationship with the energy barrier change according to he Richardson-Dushman equation:

$$\text{Gain} \propto \exp\left(-\frac{\Delta\varphi}{kT}\right) \propto \exp\left(\frac{n_t}{kT}\right), \tag{2}$$

where k is the Boltzmann constant and T is the temperature. The gain of a photodetector is the ratio of the injected hole number and the incident photon number. Control devices covered by a spun thin layer of ZnO NPs were fabricated, which is expected to generate ZnO NP rich surface as well. The control device shows an EQE of 221% and a R of 1.43 A/W at 800 nm. It induces a comparable gain improvement with that of Ar plasma etching for 20 s, which provides direct evidence that ZnO NP rich surface can enhance hole injection for a higher gain.

To determine the effect of Ar plasma etching on the device darkcurrent, the *J-V* curves of devices without Ar plasma etching, Ar plasma etched devices for 20 s or 30 s, and devices with a spun thin layer of ZnO NPs were measured in the dark, and were shown as Fig. 3(c). They all show the typical rectification behavior, indicating that the NIR photodetectors have the asymmetry characteristics. The reverse bias darkcurrent (leakage current) was reduced by about one order of magnitude after Ar plasma etching for 20–30 s or after spin-coating a thin layer of ZnO NPs at −4.5 V. The declined darkcurrent can be explained by the higher hole injection barrier height in the dark under reverse bias induced by the ZnO rich nanocomposite surfaces, which is illustrated by the energy diagram in Fig. 3(d). Due to the energy level difference, the bulk heterojunctions are formed, where PDTP-DFBT acts as electron donor and ZnO NPs work as electron acceptor. The valence band (VB) top of ZnO is −7.65 eV, which is much higher than the highest occupied molecular orbital (HOMO) level of PDTP-DFBT (−5.3 eV). After Ar plasma etching, the PDTP-DFBT at the interface of nanocomposite/electrode was removed and more ZnO NPs aggregated close to the Al electrode. A similar scenario exists by spin-coating an extra layer of ZnO NPs. The hole injection energy barrier height from Al to ZnO (3.35 eV) is much higher than that from Al to PDTP-DFBT (1.0 eV). It means that the holes injection under reverse bias will be more difficult in the dark after Ar plasma etching or ZnO NPs spin-coating.

The NIR-photodetector has been verified to act as a photodiode in the dark with a rectification contact, and as a photoconductor under illumination with an ohmic contact. In another word, the NIR-photodetector combines the merits of low noise of the photodiode and large gain of the photoconductor. Therefore, the noise currents were also measured by direct recording of the frequency dependent noise current density with a fast Fourier transform (FFT) spectrum analyzer. The current noise of the devices at different reverse bias was first amplified by a low noise current amplifier which is connected to the FFT analyzer. The bias applied for the noise measurement was −4.5 V, which is the same as the voltage used for EQE measurement. It can be seen from Fig. 4(a) that the total noise from 1 Hz to 1000 Hz is dominated by the 1/f noise because the measured noise current declined exponentially along with the logarithm of the frequency. At the frequency of 35 Hz, which is the same with the frequency

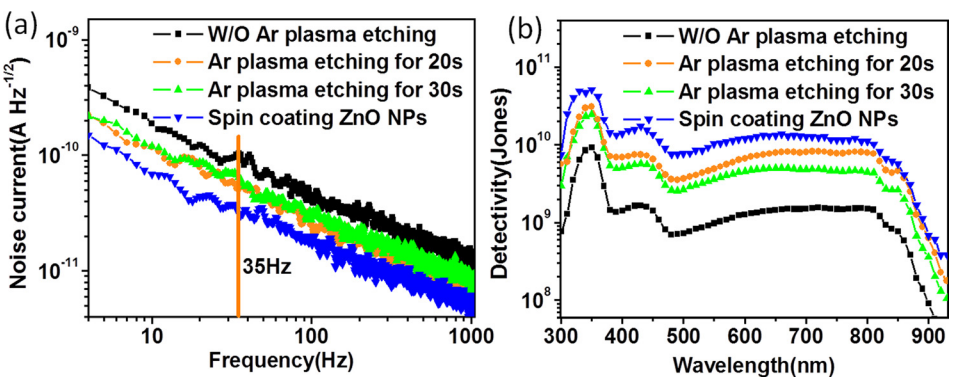

FIG. 4. For all devices at −4.5 V reverse bias. (a) The noise current curves under dark. (b) The detectivity curves.

TABLE I. Summary of the R, I_d, I_n, NEP, and D* of the devices.

Devices types	R (A/W)	I_d (mA/cm^2)	I_n (A/Hz$^{1/2}$)	NEP (W)	D* (Jones)
W/O Ar plasma etching	0.65	7.34×10^{-3}	1.04×10^{-10}	1.60×10^{-10}	1.51×10^{9}
Ar plasma etching for 20 s	1.60	2.82×10^{-4}	5.02×10^{-11}	3.14×10^{-11}	7.91×10^{9}
Ar plasma etching for 30 s	1.18	6.45×10^{-4}	6.48×10^{-11}	5.49×10^{-11}	4.45×10^{9}
Spin coating ZnO NPs	1.43	3.68×10^{-4}	3.14×10^{-11}	2.20×10^{-11}	1.11×10^{10}

applied for EQE measurement, the noise current of the devices without Ar plasma etching, Ar plasma etched devices for 20 s or 30 s, and the devices with a spun thin layer of ZnO NPs are 1.04×10^{-10} A/Hz$^{1/2}$, 5.02×10^{-11} A/Hz$^{1/2}$, 6.48×10^{-11} A/Hz$^{1/2}$, and 3.14×10^{-11} A/Hz$^{1/2}$, respectively. It is observed that the noise current decreased by about 2–3 folds in devices with excess ZnO NPs on the nanocomposite layer surfaces, which is in good accordance with the variation trend of darkcurrent. It indicates clearly that the total noise current in these photodetectors is dominated by the darkcurrent.

The detectivity (D*) is the parameter to evaluate the performance of photodetector, which is determined by

$$D^* = \frac{(AB)^{1/2}}{NEP}, \tag{3}$$

$$NEP = \frac{\overline{I_n^2}^{1/2}}{R}, \tag{4}$$

where A is the active area of device, B is the bandwidth, NEP is noise equivalent power (defined as the minimal optical signal for the signal to noise ration to be unity), $\overline{I_n^2}^{1/2}$ is the measured noise current, and R is the responsivity. The active device area is 0.06 cm^2, which is defined by the shadow masks. The corresponding wavelength dependent D* are calculated according to Eqs. (3) and (4), and are shown in Fig. 4(b). All the device parameters, including R, I_d, I_n, NEP, and D*, are summarized in Table I. The D* of devices without Ar plasma etching, Ar plasma etched devices for 20 s or 30 s, and devices with a spun thin layer of ZnO NPs are 1.51×10^{-9} Jones, 7.91×10^{9} Jones, 4.45×10^{9} Jones, and 1.11×10^{10} Jones, respectively. The specific detectivity increased about 5.2 times after Ar plasma etching for 20 s, increased about 7.4 times after spin-coating a thin layer of ZnO NPs. The dramatically improved D* resulted from the combination of the increased gain and the reduced noise, simultaneously induced by ZnO NPs rich nanocomposite surface.

In summary, we demonstrated the surface treatment of active layer can effectively enhance trap induced secondary hole injection by Ar plasma etching. The darkcurrent was diminished about one order of magnitude due to the higher hole injection barrier height. The gain was improved by 2–3 times owing to enhanced trap induced hole injection under illumination, which resulted in a high D* of 1.11×10^{10} Jones. Spin-coating ZnO NPs layer on the top of nanocomposite provided a direct evidence that excess ZnO NPs between nanocomposite and electrode can enhance hole injection under illumination. This method is general in that it can enhance the sensitivity of all type of nanocomposite photodetectors in respective to the absorption wavelength of the polymers.

This work was supported by Office of Naval Research (ONR, Grant No. N000141210556) and U.S. Defense Threat Reduction Agency (DTRA, Award No. HDTRA1-10-1-0098).

[1]L. Ma, W. Hu, Q. Zhang, P. Ren, X. Zhuang, H. Zhou, J. Xu, H. Li, Z. Shan, X. Wang, L. Liao, H. Q. Xu, and A. Pan, Nano Lett. **14**, 694 (2014).
[2]G. Konstantatos, M. Badioli, L. Gaudreau, J. Osmond, M. Bernechea, F. P. Garcia de Arquer, F. Gatti, and F. H. Koppens, Nat. Nanotechnol. **7**, 363 (2012).
[3]J. Tang and E. H. Sargent, Adv. Mater. **23**, 12 (2011).
[4]S. Z. Bisri, C. Piliego, M. Yarema, W. Heiss, and M. A. Loi, Adv. Mater. **25**, 4309 (2013).
[5]D. Ali and C. J. K. Richardson, Appl. Phys. Lett. **105**, 031116 (2014).
[6]K. Szendrei, M. Speirs, W. Gomulya, D. Jarzab, M. Manca, O. V. Mikhnenko, M. Yarema, B. J. Kooi, W. Heiss, and M. A. Loi, Adv. Funct. Mater. **22**, 1598 (2012).
[7]Y. Yao, Y. Liang, V. Shrotriya, S. Xiao, L. Yu, and Y. Yang, Adv. Mater. **19**, 3979 (2007).
[8]X. Gong, M. Tong, Y. Xia, W. Cai, J. S. Moon, Y. Cao, G. Yu, C. L. Shieh, B. Nilsson, and A. J. Heeger, Science **325**, 1665 (2009).
[9]X. Gong, M. Tong, S. Park, M. Liu, A. Jen, and A. J. Heeger, Sensors **10**, 6488 (2010).
[10]E. C. Chen, C. Y. Chang, J. T. Shieh, S. R. Tseng, H. F. Meng, C. S. Hsu, and S. F. Horng, Appl. Phys. Lett. **96**, 043507 (2010).
[11]T. K. An, C. E. Park, and D. S. Chung, Appl. Phys. Lett. **102**, 193306 (2013).
[12]F. Guo, B. Yang, Y. Yuan, Z. Xiao, Q. Dong, Y. Bi, and J. Huang, Nat. Nanotechnol. **7**, 798 (2012).
[13]F. Guo, Z. Xiao, and J. Huang, Adv. Opt. Mater. **1**, 289 (2013).
[14]R. Dong, C. Bi, Q. Dong, F. Guo, Y. Yuan, Y. Fang, Z. Xiao, and J. Huang, Adv. Opt. Mater. **2**, 549 (2014).
[15]Y. Fang, F. Guo, Z. Xiao, and J. Huang, Adv. Opt. Mater. **2**, 348 (2014).
[16]X. Hu, Y. Dong, F. Huang, X. Gong, and Y. Cao, J. Phys. Chem. C **117**, 6537 (2013).
[17]X. Hu, K. Wang, C. Liu, T. Meng, Y. Dong, S. Liu, F. Huang, X. Gong, and Y. Cao, J. Mater. Chem. C **2**, 9592 (2014).
[18]J. Qi, X. Zhou, D. Yang, W. Qiao, D. Ma, and Z. Y. Wang, Adv. Funct. Mater. **24**, 7605 (2014).
[19]J. You, L. Dou, K. Yoshimura, T. Kato, K. Ohya, T. Moriarty, K. Emery, C. C. Chen, J. Gao, G. Li, and Y. Yang, Nat. Commun. **4**, 1446 (2013).